Journal of Mathematical Chemistry 10(1992)183–204 

# CONTINUUM MODELS OF ENVIRONMENTAL EFFECTS ON MOLECULAR STRUCTURE AND MECHANISMS IN CHEMISTRY AND BIOLOGY

Stanislav MIERTUS*
*International Centre for Pure and Applied Chemistry, UNIDO, Area di Ricerca, Padriciano 99, 34012 Trieste, Italy*

and

Vladimir FRECER☆
*Department of Physiology and Biophysics, Mount Sinai School of Medicine, City University of New York, 1 Gustave L. Levy Place, New York, NY 10029, USA*

## Abstract

In this paper we briefly review the methodologies of environmental effects with emphasis on continuum solvent effect models and on interphase partitioning. We also focus attention on simpler methods that are easily applicable to larger models of complex biological processes. The applications of the described methods to various problems in chemistry and biology are listed, and selected examples of application of the methods on the description of environmental effects are given.

## 1. Introduction

Environmental effects play an important role in the major part of mechanisms in chemistry and are often decisive in subtle biological processes. Therefore, recent research in theoretical chemistry is more and more oriented towards the development of appropriate methodologies capable of describing these effects (see e.g. review papers [1–3]).

Environmental effects in a condensed medium can be considered not only as the effect of solvent (which is naturally the most common case), but can further comprise more complex phenomena like mixed solvents; ion (salt) effects; specific effects of structured components (such as biomacromolecular chains, interphase boundaries, membranes, microsurfaces of micelles, etc.).

This complexity is often a barrier for the exact description of phenomena and leads to simplifications in the models used. Moreover, at present – despite the rapid development of computer techniques – there is a necessity to find a proper compromise between the exactness of the method and the complexity of the model.

* Permanent address: Faculty of Chemistry, Slovak Technical University, 81237 Bratislava, Czechoslovakia.
☆ Permanent address: Cancer Research Institute, Slovak Academy of Sciences, 81232 Bratislava, Czechoslovakia.

Several different approaches of solvent effect evaluation have been developed in many laboratories (see refs. cited in section 2). In the present paper we will shortly review mainly the methodologies of environmental effect description developed in our laboratory. We will focus prevailingly on continuum models and we will try to present their capabilities and limits in the description of:

(i) solvent effects (including effects on very large solute systems);
(ii) partitioning and transport through interphase boundaries;
(iii) reactivity and dynamics in solutions (in combination with appropriate dynamic models).

We will then briefly present some selected examples of application of the reviewed methodologies of environmental effect description.

## 2. Methodologies of environmental effect description

Several groups of methods for environmental effect description have been developed up to now, ranging from discrete solvent quantum mechanical models [4–6] to continuum or hybrid quantum mechanical models [7–12], Langevin dipole type models [13], continuum classical models [14–18], classical statistical models such as Monte Carlo [19–21], molecular dynamics [22–25], and free energy perturbation treatment [26,27]. Any of these methods has its own pros and cons. Generally, discrete quantum mechanical models are fully capable of describing the principal energetic properties of the interaction between solute and solvent molecules (including charge transfer). They are, however, limited to smaller solute molecules, as well as to the consideration of a restricted number of solvent molecules. Moreover, there are extreme computer needs for the optimization of the solvent molecule configuration; therefore, such methods could be predominantly used for the evaluation of local specific effects in the solvation (such as strong hydrogen bonding or hydrogen transfer mediated by water molecules) rather than for the simulation of overall solvent effects.

Classical statistical models (molecular dynamics or Monte Carlo) can properly describe the statistical behaviour of solvated systems; however, description of the changes in the electronic structure of the solute during solvation is still difficult to approach properly. Moreover, discrete models, as well as statistical ones, are also faced with problems of description of the boundary with the bulk, where the simulation of the rest of the solvent (i.e. bulk) has not been well settled yet.

Continuum models are suitable for the description of bulk environmental effects. They allow us to study also large solvated solute systems, including the combination with a quantum chemical description of the intrinsic part. The lack of possibilities to properly describe specific solute–solvent interactions by means of continuum models can be overcome by combining them with discrete models [28].

There are other numerous possibilities of applications of continuum models, especially for large systems [2–4,18], partitioning between two phases [29–33], etc.

## 2.1. SOLVENT EFFECT WITHIN CONTINUUM MODELS

The continuum models [7,10–12,14–18] consider the solvent to be an infinite continuous dielectric medium possessing the macroscopic characteristics (such as dielectric constant, mean polarizability, etc.) of the pure liquid. The solute is placed into a cavity in the continuum and solute–solvent interactions are treated either classically or quantum mechanically. The solution process thus consists of inserting a solute molecule into a suitable cavity (spending energy of cavitation for its creation) and "switching on" the interactions with surrounding solvent molecules. This interaction involves the electrostatic (i.e. the Coulombic and polarization) interaction, as well as the dispersion and repulsion interaction contributions. The overall change of the Gibbs free energy of solvation $\Delta G_{solv}$ in the continuum models is generally evaluated [12,33] as a sum of all these terms:

$$\Delta G_{solv} = \Delta G_{elst} + \Delta G_{rep} + \Delta G_{disp} + \Delta G_{cav} + \Delta G_{phas} . \quad (1)$$

The last term in eq. (1), $\Delta G_{phas}$, is related to the positional entropy changes that occur during the solution process [32,33]. Some authors [35] do not include the $\Delta G_{rep}$ term, arguing that this term is already included in the cavitation Gibbs free energy $\Delta G_{cav}$ calculation. In our opinion, $\Delta G_{cav}$ includes only the energy spent for the creation of free space for the solute molecule in the solvent. After the insertion of the solute into the cavity, all such interactions should be taken into account (including the repulsive one).

In recent years, much effort has been devoted to the elaboration of methods for calculating the electrostatic part of the solvation Gibbs free energy, but relatively less effort has been given to the description of the remaining contributions [2,34,35].

Below, we will shortly review the approaches for the evaluation of individual energetic contributions with the focus on those developed in our laboratory.

### *2.1.1. Electrostatic contribution to solvent effect within continuum models*

The electrostatic term in continuum models can be calculated with the aid of diverse methods ranging from simple estimates to the sophisticated quantum mechanical treatments. An approximate estimate of the Coulombic part of the electrostatic Gibbs free energy of the solute–solvent interactions can be easily obtained via a simple expression, which was later modified [60] as follows:

$$G_{elst} = \tfrac{1}{2}\sum_{i,j} Q_i q_j / r_{ij} = -\tfrac{1}{2}(\varepsilon - 1)/\varepsilon \sum_{i,j} Q_i Q_j / r_{ij} , \quad (2)$$

where $r_{ij}$ is approximated as $r_{ij} = d_{ij} + r^{i}_{vdw}$, $d_{ij}$ is the interatomic distance (for details, see refs. [60]), $\varepsilon$ is the relative permittivity of the solvent, and $Q_i$, $Q_j$ are solute atomic net charges. For the case of simple ions, eq. (2) leads to the well-known Born formula for solvation Gibbs free energy [1].

It can also be computed using the simplest "solvaton" model [61,62]. This solvaton model is based on the simple representation of induced charges in solvent by charges called solvatons $q'_i$. Each solvaton $q'_i$ is associated with individual atomic charges of solute $Q_i$, and solvation properties are evaluated by solving Hartree–Fock equations with the perturbed Hamiltonian, namely,

$$H_e = H_0 + \sum q'_i/(r - r_i). \tag{3}$$

The disadvantage of the solvaton model consists of the rather approximate evaluation of the solvaton charges $q'_i$.

These quantities should be evaluated more sophistically – based on the polarization of solvent dielectrics by solute electric field. Therefore, we later developed a hierarchy of methods based on the Polarizable Continuum Model (PCM) [10–12] at the ab initio level, where the solvent charge distribution $\sigma(s)$ spread over the cavity surface $S$ is determined via numerical solution of a Laplace equation for the polarization of the dielectric medium at the cavity boundaries [10,11]:

$$\sigma(s) = -P_0 n\sigma_+ = \frac{\varepsilon - 1}{4\pi}\left(\frac{\partial V_{tot}(s)}{\partial n}\right)_{s^+} = -\frac{\varepsilon - 1}{4\pi\varepsilon}\frac{\partial}{\partial n}\left[V_\rho(s) + V_\sigma(s)\right]_{s^-}, \tag{4}$$

where $V_\rho(s)$ and $V_\sigma(s)$ are the electrostatic potential contributions, related to the solute and solvent charge distribution functions $\rho(r)$ and $\sigma(s)$, at the cavity surface point $s$ just inside the cavity, and $\varepsilon$ is the solvent permittivity. Equation (4) is solved iteratively taking into account solvent–solvent polarization. Based on the final solvent charge density $\sigma(s)$, a charge density (reaction field-like) $V_\sigma$ operator can be evaluated as follows:

$$V_\sigma = \int_S \frac{\sigma(s)}{|r - s|}\,dr = \sum_i^M \frac{q_i}{|r - r_i|}. \tag{5}$$

The electrostatic solute–solvent interaction is then calculated via the Hamiltonian of the solute $H_0$ and the $V_\sigma$ operators:

$$\Delta E_{elst} = [\langle \Psi_R | H_0 + V_\sigma | \Psi_R \rangle + E^{nucl}] - [\langle \Psi_0 | H_0 | \Psi_0 \rangle + E_0^{nucl}]; \tag{6a}$$

the Gibbs free energy contribution $\Delta G_{elst}$ can then be evaluated as follows (see detailed discussion in refs. [32,45]):

$$\Delta G_{\text{elst}} = \Delta E_{\text{elst}} - \tfrac{1}{2}[\langle \Psi_R | V_\sigma | \Psi_R \rangle - \int \rho^{\text{nucl}}(\boldsymbol{r}) V_\sigma(\boldsymbol{r}) \mathrm{d}\boldsymbol{r}], \tag{6b}$$

where $\Psi_0$ and $\Psi_R$ are the wave functions of the isolated and solvated molecule. Since $V_\rho(s)$ and $V_\sigma(s)$ depend in the quantum mechanical model on the solvent charge distribution $\sigma(s)$ and on $\rho(\boldsymbol{r})$, eqs. (4)–(6) have to be solved iteratively by numerical integration over the complex shape of the boundary surface [10].

The original ab initio version of the PCM model was modified to a variety of simplified methods that are easily applicable also to large bioactive molecules or polymers. These modifications include (i) a simplified description of the solvent influence upon the solute, (ii) modification of the $\Delta G_{\text{elst}}$ calculation into the semiempirical quantum chemical level, or (iii) a classical (discrete charge distribution type) calculation suitable for biopolymers.

The first type of modification involves the definition of the reaction field operator $V_\sigma$, where the induced solvent charge density $\sigma(s)$ is in the simplified version taken constant over the surface of each free atomic Van der Waals sphere and the solvent influence is then simulated via a small number of representative point charges $q_i$ (eq. (5)) located in the points of local electrostatic potential extremes (the so-called reduced PCM model [63]).

Another so-called classical version of the PCM model including solute–solvent, solvent–solvent and solvent–solute polarizations has recently been elaborated [18]. This model is particularly suitable for the treatment of the solvent effect on large biomacromolecules. In order to introduce a classical description of the solute–solvent polarization in the version of the PCM model for biopolymers, we have implemented several modifications. We have assumed a discrete multipole representation of the solute $\{Q_i, \boldsymbol{m}_i\}$ centered on the atomic nuclei, as has been suggested before by other authors [9, 16, 65] (we neglected induced moments higher than dipoles). The representation of the solvent charge density $\sigma(s)$ is evaluated by the same strategy as in the polarizable continuum model [10]. The expression for the electrostatic solute–solvent interaction Gibbs free energy then takes the form:

$$\Delta G_{\text{elst}} = \tfrac{1}{2}\sum_i Q_i V_i - \tfrac{1}{2}\sum_i \boldsymbol{m}_i \cdot \boldsymbol{E}_i \ldots , \tag{7}$$

where $Q_i$ are the net atomic charges of the biopolymer (e.g. coming from an ab initio calculation on a fragment of the biopolymer [64]), and $\boldsymbol{m}_i$ are induced dipoles obtained from the mutual polarization of the fragments combined to form the biopolymer structure [65]* and from polarization of the solute by the solvent charge distribution. The medium is characterized by the relative permittivity $\varepsilon_+$, which is constant at

*Since the polarization of point dipoles in the classical charge distribution representation is not bound and can diverge at shorter distances, the model of "smeared out" dipoles should be used to avoid infinite polarization by the fragments at close distances instead of cut-off. Precise forms of potential and field functions at short distances are given in the original work of Thole [65a].

any point of the boundary surface $s$, and the dielectric properties of the space inside the cavity walls are usually represented by a low polarity dielectric $\varepsilon_-$ (usually equal to 1).

First iteration for the solvent charge distribution $q_k^{(0,0)}$ is then computed similarly to the original exact model [10,12] at the surface element with area $S_k$ as follows:

$$q_k^{(0,0)} = \sigma_k^{(0,0)} S_k = -1/4\pi[(\varepsilon_+ - \varepsilon_-)/\varepsilon_+] S_k \sum_i [Q_i r_{ki}/(\varepsilon_- r_{ki}^3) + \boldsymbol{m}_i^{(0,0)}/(\varepsilon_- r_{ki}^3) - 3(\boldsymbol{m}_i^{(0,0)} \cdot \boldsymbol{r}_{ki}) r_{ki}/(\varepsilon_- r_{ki}^5)] \cdot \boldsymbol{n}_k . \tag{8}$$

Then, within the iterative solution of the Poisson equation, the effect of solvent–solvent polarization of induced charge distribution $[q_k^{(0,t)}]$ is introduced in a similar way as in our original model [10,12] using an iterative procedure (running over index $t$) via the following expression:

$$q_k^{(0,t)} = q_k^{(0,0)} - 1/4\pi[(\varepsilon_+ - \varepsilon_-)/\varepsilon_+] S_k \boldsymbol{E}_k^{s(0,t-1)} \cdot \boldsymbol{n}_k + \tfrac{1}{2}[(\varepsilon_+ - \varepsilon_-)/\varepsilon_+ \varepsilon_-] q_k^{(0,t-1)} [1 - (S_k/(4\pi(r_{\mathrm{vdw}}^k)^2)^{1/2}], \tag{9}$$

where

$$\boldsymbol{E}_k^{s(0,t-1)} = \sum_{j \neq k} q_j^{(0,t-1)} \boldsymbol{R}_{kj}/(\varepsilon_- R_{kj}^3) \quad \text{and} \quad t = 0, \ldots, f. \tag{10}$$

The solvation Gibbs free energy including solute–solvent polarization, as well as solvent–solvent self-polarization, at this step is evaluated according to eq. (7), namely as:

$$\Delta G_{\mathrm{elst}}^{(0,f)} = \tfrac{1}{2} \sum_i Q_i V_i^{s(0,f)} - \tfrac{1}{2} \sum_i \boldsymbol{m}_i^{(0,0)} \cdot \boldsymbol{E}_i^{s(0,f)}, \tag{11}$$

where

$$V_i^{s(0,f)} = \sum_k q_k^{(0,f)}/(\varepsilon_- R_{ik}) \tag{12}$$

and

$$\boldsymbol{E}_i^{s(0,f)} = \sum_k q_k^{(0,f)} \boldsymbol{R}_{ik}/(\varepsilon_- R_{ik}^3) \tag{13}$$

are the solvent potential and field from the solvent charge distribution $\sigma(s)$ at the site of solute atom $i$, respectively.

The above described procedure can be coupled with the solvent–solute back-polarization which will modify the solute charge distribution $\rho(r)$ under the influence

of the solvent charge distribution $\sigma(s)^{(0,f)}$.* The new solute charge distribution $[Q_i, \boldsymbol{m}_i^{(p,f)}]$ is evaluated in a major iterative cycle running over index $(p)$ and containing the inner cycle running over index $(t)$. The new solute charge distribution is therefore:

$$\boldsymbol{m}_i^{(p+1,0)} = \alpha_i \boldsymbol{E}_i^{(p,f)}, \tag{14}$$

where

$$\boldsymbol{E}_i^{(p+1,t+1)} = \sum_{j\neq i} Q_j \boldsymbol{r}_{ji}/(\varepsilon_- r_{ji}^3) + \sum_{j\neq i} [\boldsymbol{m}_j^{(p+1,t)}/(\varepsilon_- r_{ij}^3) - 3(\boldsymbol{m}_j^{(p+1,t)} \cdot \boldsymbol{r}_{ij})\boldsymbol{r}_{ij}/(\varepsilon_- r_{ij}^5)] + \sum_k q_k^{(p,f)} \boldsymbol{R}_{ik}/(\varepsilon_- R_{ik}^3) \quad t = 0, \ldots, f. \tag{15}$$

$\alpha_i$ denotes here the isotropic atomic polarizability [65].

The inner iterative cycle is then repeated starting from the new solute charge distribution, and a new set of solvent charges $q_k^{(p+1,0)}$ is obtained as:

$$q_k^{(p+1,0)} = -1/(4\pi)(\varepsilon_+ - \varepsilon_-)/\varepsilon_+ S_k \sum_i [Q_i \boldsymbol{R}_{ki}/(\varepsilon_- R_{ki}^3) + \boldsymbol{m}_i^{(p+1,f)}/(\varepsilon_- R_{ki}^3) - 3(\boldsymbol{m}_i^{(p+1,f)} \cdot \boldsymbol{R}_{ki})\boldsymbol{R}_{ki}/(\varepsilon_- R_{ki}^5)] \cdot \boldsymbol{n}_k, \tag{16}$$

resulting in a new set of mutually polarized solvent charges $q_k^{(p+1,f)}$ (eqs. (9), (10)) and continues with the next back-polarization step (eqs. (14), (15)), etc. for $p = 1, \ldots, f$ until complete self-consistency is reached $(f,f)$, usually for $(p, t) \leq 5$. At the end of the double iterative procedure, the self-consistent solvent charge distribution $\{q_k^{(f,f)}\}$ is compensated to achieve the exact theoretical value of the total induced solvent charge $q_{\text{tot}} = -(\varepsilon_+ - \varepsilon_-)/\varepsilon_+ Q_{\text{tot}}$, where $Q_{\text{tot}}$, $q_{\text{tot}}$ are the sums of solute atomic charges and solvent charges, respectively, as:

$$q_k^{(f,f)'} = q_k^{(f,f)} - 1/n \left[ \sum_{l=1}^{n} q_l^{(f,f)} + (\varepsilon_+ - \varepsilon_-)/\varepsilon_+ \sum_{i=1}^{N} Q_i \right]. \tag{17}$$

The Gibbs free energy of the electrostatic solute–solvent interaction is then finally computed using eq. (7) as:

$$\Delta G_{els}^{(f,f)} = \tfrac{1}{2} \sum_i Q_i V_i^{s(f,f)} - \tfrac{1}{2} \sum_i \boldsymbol{m}_i^{(f,f)} \boldsymbol{E}_i^{s(f,f)}, \tag{18}$$

*Matrix formulation of a discrete problem [9,65], similar to the presented iterative formulation of classical continuum solvent effect description, shows that the convergence of the solute–solvent self-consistent field depends upon the actual choice of atomic coordinates, $Q_i$, $a_i$ and $r_{ivdw}$. Further tests on a wider series of solutes and solvents of different structure and polarity will reveal the limits of applicability of the iterative evaluation of the solvent–solute back-polarization.

where $\{Q_i, \boldsymbol{m}_i^{(f,f)}\}$ and $\{q_k^{(f,f)}\}$ are the final self-consistent, mutually polarized solute and solvent charge distributions in the classical representation.

The alternative class of modifications is related to a simplified calculation of the molecular electrostatic potential from a ZDO type wave function [80] (the semiempirical EPCM version [63]). The Gibbs free energy of electrostatic solute–solvent interaction is then calculated classically (eq. (7)).

### 2.1.2. *Nonelectrostatic contributions*

#### (a) *Dispersion and repulsion energy*

Our concept [34] is based on the London [36–38] and Born [39] formulae for long-range dispersion and repulsion-energy constributions. If we consider a solute molecule in a spherical cavity with radius $r_{so}$ surrounded by $N$ spherical solvent molecules with radii $r_{sv}$ forming the first solvation shell placed at an equilibrium distance $r_{so} + r_{sv}$ from the centre of the solute, we can easily obtain a combined expression involving both forces (with restriction on the first expansion terms only):

$$E_{\text{disp,rep}} = E_{\text{disp}} + E_{\text{rep}} = -\frac{C_{ij}}{r_{ij}^6} + \frac{B_{ij}}{r_{ij}^{12}}; \tag{19}$$

if

$$\left[\frac{\partial E_{\text{disp,rep}}}{\partial r_{ij}}\right]_{r_{ij}=r_{\text{eq}}} = \frac{\partial}{\partial r_{ij}}\left[-\frac{C_{ij}}{r_{ij}^6} + \frac{B_{ij}}{r_{ij}^{12}}\right]_{r_{ij}=r_{\text{eq}}} = 0, \tag{20}$$

then

$$E_{\text{disp,rep}}^{\text{eq}} = -\frac{1}{2}\frac{C_{ij}}{r_{ij}^6}.$$

In a real liquid, the molecules of the solvent are located in solvation shells throughout the entire volume and show macroscopic structural properties as if averaged over all the possible orientations, thereby satisfying the Boltzmann distribution. The total dispersion and repulsion interaction energy of the assembly is expressed as a sum of pair interactions $U_{(r)} = \sum_{i<j} u(\tau_i, \tau_j)$ defined for particles $i$ and $j$ via the combination of London [36–38] and Born [39] formulae using experimental atomic quantities measured for constant $\{T, p\}$ conditions (i.e. within an isothermal–isobaric statistical ensemble); here, $\tau$ denotes the set of all coordinates. The mean Gibbs free energy of the dispersion–repulsion interaction of such an assembly is [40] given by:

$$\Delta G_{\text{disp,rep}} = \gamma \int \sum_{i<j} u(\tau_i, \tau_j)\rho^{(2)}\tau_i, \tau_j)\,\mathrm{d}\tau, \tag{21}$$

where $\gamma$ represents the number density and $\rho^{(2)}(\tau_i, \tau_j)$ is the distribution function (e.g. for an isotropic liquid of hard-core molecules). The molecular orientations of

the solvent molecules $\rho^{(2)}(\tau_i, \tau_j)$ (implicitly defined by the calculation scheme) are regarded as averaged over all orientations. In the case of the molecular representation of interacting species, we assume spherical structureless particles characterized by "averaged" molecular properties and in the atomic representation of the solute and solvent molecules, statistical averaging is done over all possible molecular orientations. The integration in eq. (21) can be approximated by a numerical summation over individual solvation shells. In the first solvation shell ($k = 1$), we can use an equation analogous to eq. (20). For other solvation shells ($k = 2, \infty$), it can easily be shown [34], using empirical 6–12 potentials, that the contribution of repulsion forces is negligible in comparison with the contribution of the dispersion (due to an $r^{-12}$ dependence as against an $r^{-6}$ one). Therefore, in all further equations, only the dispersion term is explicitly considered in the first solvation shell with a coefficient of $L = 1/2$ (from eq. (20)); for the other shells, the coefficient is $L = 1$. Using the London expression [38] for the dispersion interaction coefficient $C_{ij}$, the Gibbs free energy of these interactions in the condensed phase is given by

$$\Delta G_{\mathrm{disp,rep}} = -\tfrac{3}{2}\sum_{k}^{K} L_k N_k \alpha_{\mathrm{so}}\alpha_{\mathrm{sv}} \frac{\varepsilon_{\mathrm{so}}\varepsilon_{\mathrm{sv}}}{\varepsilon_{\mathrm{so}}+\varepsilon_{\mathrm{sv}}} \frac{1}{[r_{\mathrm{so}}+(2k-1)r_{\mathrm{sv}}]^6}, \tag{22}$$

where $\alpha_{\mathrm{so}}$ and $\alpha_{\mathrm{sv}}$ denote the mean (static) molecular polarizability of the solute (so) and solvent (sv) molecules; $\varepsilon_{\mathrm{so}}$ and $\varepsilon_{\mathrm{sv}}$ are the mean molecular excitation energies (usually taken as $\varepsilon = -2E_{\mathrm{homo}}$, cf. ref. [34]), $N_k$ is the packing number of the solvent spheres around the solute in the $k$th solvation shell, and the summation of $k$ ($k = 1, \infty$) runs over the whole volume of the liquid (assuming an equilibrium state of the whole system and neglecting the solute–solute interactions in diluted solution). The thickness of a solvation shell is taken as $2r_{\mathrm{sv}}$. This simple molecule–molecule approach, however, offers only a rough estimate of the dispersion–repulsion energy for solute–solvent interaction. It does not always appropriately describe the relative trends in the magnitude of $\Delta G_{\mathrm{d,r}}$ for solutes of high molecular polarizability and nonpolar liquids.

We therefore formulated [34] a hierarchy of approximate interaction formulae, passing from the molecular to the atomic level with increasing accuracy and sophistication of the description in terms of microscopic (molecular or atomic) parameters: (A) molecule–molecule type formula; (B) atom–molecule type; (C) atom–atom type; (D) atom–atom type including specific solute–solvent mutual orientations; and (E) a combination of approximations C and D (see ref. [34] for details). The appropriate formula, e.g. for approximation D, is the following:

$$\Delta G_{\mathrm{disp,rep}} = -\tfrac{3}{2}\sum_{k}^{K} L_k \sum_{i}^{T}\sum_{p}^{2}\sum_{j}^{M} \alpha_{\mathrm{so}}^{i}\alpha_{\mathrm{sv}}^{j} \frac{I_{\mathrm{so}}^{i} I_{\mathrm{sv}}^{j}}{I_{\mathrm{so}}^{i}+I_{\mathrm{sv}}^{j}} \times \frac{N_{i,k}^{D}}{[r_{\mathrm{so}}^{i}+r_{\mathrm{sv}}^{h}+t_{jh}+(p-1)d_i+(2k-2)r_{\mathrm{svf}}]^6}. \tag{23}$$

In this formula, $t_{jh}$ denotes the interatomic distance from the atom $h$ in the solvent molecule with preferred contact to solute atom $i$ [34]; $r_{sv}$ is an effective solvent radius; $d_i$ is a shielding distance; $r^i_{so}$, $r^h_{sv}$ are the atomic Van der Waals radii; $\alpha^i_{so}$, $\alpha^j_{sv}$ are the mean atomic polarizabilities; $I^i_{so}$, $I^j_{sv}$ are the atomic mean excitation energies; and $N^p_i$ is the number of solvent molecules packed around the atomic cavity surface. A detailed comparison of individual approximations can be found in ref. [34]. In this review, we present an example (see section 3) to document the dependence of $\Delta G_{d,r}$ on the level of individual approximation.

An alternative approach for the evaluation of the dispersion term of solvation Gibbs energy has recently been proposed by Floris and Tomasi [35].

(b) *Cavitation term*

For the cavitation Gibbs free energy calculations, two methods are used, namely that of Pierotti [41] and Sinanoglu [42]. However, neither is free of difficulties in the proper application to large molecules. We have modified the Pierotti approach according to Huron and Claverie [40] into an atom–molecule type formula, where the solute is represented by individual atomic spheres and the solute molecule is approximated via an effective sphere [12]:

$$\Delta G_{cav} = \sum_i^n [a(r^i_{so} + r_{sv})^2 - b(r^i_{so} + r_{sv}) + c] \frac{S^f_i}{S_i}, \tag{24}$$

where the term $S^f_i / S_i$ denotes the ratio of the free atomic Van der Waals surface and $a, b, c$ are constants for the solvent at $[T, P]$ conditions.

*2.1.3. Evaluation of molecular surface shape*

The definition of cavity boundaries in continuum models is of primary importance. The distances of polarizable solvent dielectrics from nuclei of a solute molecule strongly influence the magnitude of solvent–solute interactions. The shape of molecules has been originally defined by one sphere usually centered in the centre of mass, by atomic Van der Waals spheres with radii $r^i_{vdw}$ centered on individual atoms, or lately by the solvent accessible surface [55]. Here, the consistent set of atomic radii should be used. This problem has been dealt with in an early paper by Bondi [66], where various theoretical and experimental approaches have been taken into account in the choices of optimal values of $r^i_{vdw}$. Tomasi et al. [33] suggested to modify Bondi's atomic radii to enlarge them by approximately 20%.

We have developed a general procedure for the definition of the Van der Waals volume-shaped cavities using the structure-dependent atomic vdW radii [56]. This allows the atomic vdW spheres to vary with the actual electronic state in the solute molecules, as well as with the solvent polarity, according to

$$r^i_{vdw} = r_0 \left[ \exp(A_i q_i + B_i) + C^i_q \frac{\varepsilon - 1}{\varepsilon} q^2_i + C^i_\alpha \alpha^{1/2}_i + C^i_R \right], \tag{25}$$

where $q_i$ is the net charge, $\alpha_i$ denotes the mean polarizability, $A_i$, $B_i$, $C_q^i$, $C_\alpha^i$, and $C_R^i$ are basis set-dependent constants for an atom of type $i$. $\varepsilon$ means the solvent permittivity, and $r_0 = 1.0$ (for details, see ref. [56]).

An alternative approach for the evaluation of atomic radii has been proposed by Olivares del Valle et al. [79]. The method is based on the space integration of the electronic density of sample atoms. The above-mentioned approaches usually treat a free molecular surface which is formed by the non-overlapping part of atomic spheres. However, in the study of the solvent effect, it is often necessary to evaluate a solvent-accessible surface [31,55] which takes into account the limits of accessibility of solvent molecules to solute molecular surface, due to the actual volume of solvent molecules.

### *2.1.4. Dielectric function accounting for the effect of ionic strength*

To account for the effect of electrolyte concentration in solutions, we have used [18] and effective permittivity of the solvent $\varepsilon_+^{\text{eff}}$ (applied outside the solute boundaries) that is based on the Debye–Hückel approximation for the solution of the Poisson–Boltzmann equation. Such a dielectric function, dependent within the Debye–Hückel theory on the ionic strength of the solution and on the distance from the ion, increases the value of the solvent bulk dielectric constant $\varepsilon_b$ proportionally to the screening effect of counterions. Permittivity is commonly defined as the ratio of the potential of a charge in vacuo $V_{\text{vac}}$ to that in a dielectric medium $V_{\text{med}}$. Since the analytical solution of the Poisson–Boltzmann equation for a $V_{\text{med}}$ potential outside the solute boundaries is not available for complex molecular cavity shapes, we use here the numerical approach for the derivation of the macromolecular potential of the solvated biopolymer described above (see section 2.1.1).

Starting with the $V_{\text{med}}$ potential for an atom in a spherical cavity of radius $r_{\text{vdw}}$ in a medium with ionic strength $I$ [77], such a definition of permittivity leads to the following expression for the dielectric function:

$$\varepsilon_+^{\text{eff}}(r) = V_{\text{vac}}(r)/V_{\text{med}}(r) = \varepsilon_b(1 + r_{\text{vdw}}/r_D)\exp[(r - r_{\text{vdw}})/r_D], \tag{25a}$$

where

$$r_D = [\varepsilon_b RT/(2F^2 I)]^{1/2} \tag{25b}$$

is the Debye length, $r$ is the distance from the atom, $R$ means the gas constant, $T$ is the temperature, and $F$ represents the Faraday constant. The effective permittivity $\varepsilon_+^{\text{eff}}$ approaches the value of the bulk solvent dielectric constant $\varepsilon_b$ as the ionic strength decreases to zero and as the distance $r$ from the atom vanishes. On the other hand, it increases over the $\varepsilon_b$ value with increasing distance $r$ since the potential of a charged atom will be screened more effectively in the presence of counterions. The use of effective permittivity will increase the screening effect of the solution at the cavity boundaries assuming a mean effect of the counterion field [78] similar to that in the linear Poisson–Boltzmann equation. For example, at the atomic Van

der Waals boundaries ($r = r_{vdw}$ ranging from 1.44 Å to 2.05 Å for H to Cl [32]) in water ($\varepsilon_b = 78.5$) at 298.15 K and physicological concentration (0.145 M) of a univalent (1:1) electrolyte (e.g. NaCl), where the Debye length is approximately equal to 8.0 Å, the relative effective permittivity $\varepsilon_+^{eff}$ will vary in the interval from 92.6 to 98.6. For further details, see [18].

## 2.2. MODELLING OF PARTITIONING AND TRANSPORT THROUGH INTERPHASE BOUNDARIES WITHIN CONTINUUM MODELS

The above described polarizable continuum model was originally developed for the evaluation of the homogeneous solvent effect. However, another phenomenon, namely the partitioning between two immiscible phases or the transport through a boundary which separates two such liquid phases, can also be represented [29,30,43,45].

The interphase partition coefficient can be calculated via the difference of solvation Gibbs free energies $\Delta G^1_{solv}$, $\Delta G^2_{solv}$ [30] as:

$$\log P = -\frac{\Delta G^{1,2}_{part}}{2.3RT}, \tag{25c}$$

where $\Delta G^{1,2}_{part} = \Delta G^1_{solv} - \Delta G^2_{solv}$ is the partition Gibbs energy. Usually, $\log P_{1,2}$ is evaluated for the octanol–water system, which requires the calculation of the individual $\Delta G$ components for both solvents [30]. Usually, eq. (25c) is not used in an absolute sense, but relative trends, i.e. $\log P_{1,2} = a\Delta G^{1,2}_{part} + b$, are compared for a series of molecules [29,30] (see also section 3).

A similar approach has been applied for more complex partitioning phenomena as liquid–liquid (or gas–liquid) chromatography [30,46] based on the assumption that the separation process is ruled mainly by partitioning between stationary and mobile phases. The key parameter, i.e. the capacity ratio $k_{m,s}$, can be evaluated accordingly:

$$\log k_{m,s} = a'\Delta G^{m,s}_{part} + b', \tag{26}$$

where $\Delta G^{m,s}_{part}$ is calculated again as the difference of solvation Gibbs energies in mobile and stationary phases [30]. For example, for reverse phase liquid chromatography (RP HPLC) we have modelled the mobile phase water–methanol mixture by means of the continuum model for the water solvent, and the nonpolar stationary C18 phase has been represented by octanol (or octanol–hexane mixture) [47].

The theoretically evaluated log $P$ values enable also the rough estimation of the probability of reaching the site of metabolic activation or the crucial biological interaction target and the deduction of implications for the relative potency within series. This is usually done via a QSAR approach, where experimental biological activities of the series of compounds are correlated with theoretically evaluated log $P$ by the above-mentioned approach [44].

It is clear that the partitioning and especially the transport in complex chemical or biological media composed of several phases and interphase boundaries need appropriate models which take into account important features of reality.

Some of them can be represented also in continuum models. For example, our original polarizable continuum model which was elaborated for a homogeneous solvent environment can be easily extended to the case where the solute cavity surrounding space is composed of subspaces with different permittivites ($\varepsilon_r$) [43,48]. We further extended this model considering an electric bilayer between two phases (fig. 1) [43]. The electric bilayer is represented by a two-dimensional mesh of point

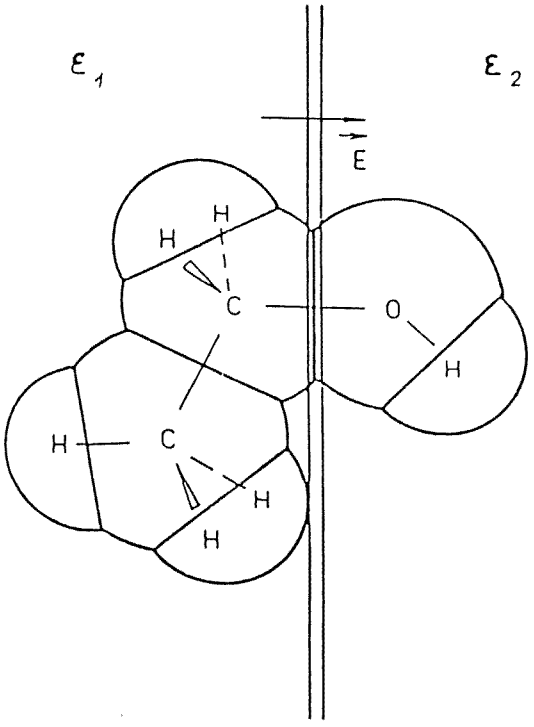


Fig. 1. Model of transition path of an ethanol molecule when passing the nonpolar/polar phase boundary ($\varepsilon_1$ cotanol, $\varepsilon_2$ water).

dipoles which are included in the solute Hamiltonian. Thus, the energetic profile of the transport process through such a boundary can be evaluated, as well as the kinetics of the transport.

The kinetics of such a process, assuming the compartment model of the biosystem composed of a series of polar and nonpolar phases, obey for a polar to nonpolar (p–n) phase transition the equation:

$$-\frac{\partial c_p}{\partial t} = k_p c_p, \tag{27}$$

where $c_p$ denotes the concentration in the phase p and $k_p$ is the rate constant. It can be estimated via the activation Gibbs free solvation energy $\Delta G^{\neq}_{solv}(p \rightarrow n)$ of the transition of the compound from phase p to n [43] as:

$$k_p = A \exp\left(-\Delta G^{\neq}_{solv}(p \rightarrow n)/RT\right), \tag{28}$$

where $A$ is a pre-exponential factor, and $\Delta G^{\neq}_{solv}(p \rightarrow n) = \Delta G^{*}_{solv} - \Delta G^{p}_{solv}$ and $\Delta G^{*}_{solv}$ represent the solvation Gibbs free energy of the molecule when passing the phase boundary which is simulated by an electric field gradient and two solvents surrounding the relevant parts of the molecule [43] (fig. 1).

Theoretically evaluated $\log P_{p,n}$, $k_p$, $k_n$ quantities allow the estimate of the probabilities of reaching the metabolic activation site or the receptor of crucial biological interaction for the parent bioactive molecules and their metabolities and stimulate deductions for the relative potency determinants within the structure activity analyses of bioactive compounds [44].

## 2.3. CONTINUUM MODELS FOR INTERPRETATION OF MOLECULAR REACTIVITY AND DYNAMICS IN SOLUTION

The above-mentioned polarizable continuum models can be applied for the interpretation of various types of molecular properties. One of the most important fields of application is the reactivity of molecules, which includes searching initial, transition and final states as well as reaction path, usually by quantum mechanics methods. While most reactions take place in condensed media, the solvent effect often plays an important role. Continuum models have been successfully used for the simulation of the solvent effect on reactivity (see e.g. [49]). When applying these methods, it should be kept in mind that the calculation of the energy of the system at each point of the energetical hypersurface should include solute–solvent interactions. The problem is quite time-consuming since for any change of geometry (e.g. each point searching of optimal geometry or reaction path), the molecular cavity surface is to be redefined and the new set of self-consistent charges is to be calculated. Naturally, the re-definition can be done manually. However, sophisticated approaches which include the solute–solvent interactions directly in the minimization energy or the reaction path searching have recently been proposed [50].

Sometimes the solvent plays an important role not only as an environmental field but some solvent molecules are involved in the reaction mechanism (e.g. water molecule mediating proton transfer). In such cases, we have adopted [28,51] a combined, i.e. discrete–continuum, model. Here, the intrinsic solvent molecules are considered as part of the "solute" and the rest of the bulk solvent is simulated by continuum models.

Recently, we have extended the PCM model to be capable of describing dynamic features of the solvent during molecular processes in solution, namely fluctuations of the solvent [82] and dielectric friction of the solvent [83].

Another field where continuum models have recently been considered is molecular dynamics. This might appear strange at first sight because, as is well

known, molecular dynamics of solvated systems is based on equations of motion of discrete molecules of solvent surrounding the solute. However, as we mentioned in the introduction, such models can suffer from the absence of a bulk surrounding the solvated complex. This could be overcome by using continuum models, at least in the two following ways:

(i) The charges of atoms of solvent molecules which are exposed to the bulk are scaled [52,53] to resemble solvated atoms in bulk, i.e. only a modified set of charges is used. This scaling could be done either arbitrarily or by using the procedure of the classical version of PCM (see section 2.1.2).

(ii) Force field evaluation of $E_p$ in molecular dynamics is extended by the following terms:

$$E_p^{tot} = E_p^{discr} + E_p^{discr-bulk}, \tag{29}$$

where $E_p^{discr}$ is the standard force field evaluation of potential energy [54] of discrete particles in molecular dynamics (solute + solvent molecules); $E_p^{discr-bulk}$ is represented by a similar approach as in the classical PCM model (section 2.1.1) [53]. In this procedure, atomic surfaces of solvent molecules to the bulk are evaluated by means of an efficient analytical procedure. For each atom, the corresponding solvent charge is evaluated and the corresponding interaction energy of the "discrete" atom with bulk surface charges is also evaluated. These various tests of procedure are now in progress [53].

## 3. Applications

The above described methodology of continuum models has been applied in the research of various problems in chemistry and biology. Its main areas of application are the following:

(i) molecular properties of solute in condensed medium and energetics of solvation [31,33,34,45,67];

(ii) molecular structure and conformations in solutions [44,68,70];

(iii) electronic absorption and emission process [28,62];

(iv) photochemical process [71];

(v) weak intermolecular interactions [72];

(vi) mechanisms of chemical reactions in condensed phase [44,49];

(vii) interphase partitioning [29,30,57,73];

(viii) interpretation of chromatographic data [46,47];

(ix) modelling of interphase partitioning and transport of molecules in a biosystem [43–45,74];

(x) mechanistic studies into their metabolic activation pathways (biotransformation) [44,75];

(xi) interactions of ultimate drug species with biopolymers (nucleic acids, enzymes, etc.) [31,68,76];

(xii) modelling of solvent bulk properties at molecular dynamics calculations [53];

and others.

Here we present only some selected examples of the applications which can document the possibilities and limits of the above-mentioned methodology.

### 3.1. COMPARISON OF THE CLASSICAL PCM MODEL TO THE ORIGINAL AB INITIO PCM MODEL

Various applications of the recently elaborated classical PCM model [18] which is described in section 2.1.1 are now in progress, ranging from solvation of drug-DNA complxes, $pK_a$ calculation for solvated proteins, simulation of bulk solvent in molecular dynamics, etc. Here we mention only some examples of calculations on solvation, which naturally cannot serve as a complete proof of the adequacy of the presented method, but can rather illustrate a first experience with the method of the classical PCM model.

We have completed the calculation of the electrostatic contribution to solvation Gibbs free energy within the classical PCM, as well as the original ab initio PCM model [11] on *cis* (C) and *trans* (T) forms of N-methyl-N-nitrosurea (MNU) and N-ethyl-N-nitrosurea (ENU) in water. The results of the calculations performed in the STO-3G basis set using optimized geometry (by the AM1 method [81]) are shown in table 1, together with the results obtained with the classical model presented in section 2.1.1 [18]. More polar *cis* forms of nitrosureas are, in both methods, more

Table 1

Comparison of quantum mechanical and classical solvent effect calculations (all quantities are in [kcal/mol]).

| Molecule | $\Delta G_{els}^{(f,f)}$ (ab initio)[a] | $\Delta E_0$[b] | $\Delta G_{els}^{(f,f)}$ (class.)[c] |
|---|---|---|---|
| MNU–*trans* | −5.41 | −6.49 | −4.72 |
| MNU–*cis* | −7.80 | | −5.02 |
| ENU–*trans* | −5.39 | −6.47 | −4.70 |
| ENU–*cis* | −7.23 | | −4.93 |

[a] Ab initio Gibbs free solvation energy – electrostatic contribution (eq. (6b)).
[b] Difference in the STO-3G total energies, $\Delta E_0 = E_0(T) - E_0(C)$.
[c] Classical method (eq. (18)).

stabilized by the solvent than the less polar *trans* forms. More bulky ENU is less solvated than MNU. In the classical model AM1 optimized geometry, AM1 charges and atomic isotropic polarizabilities after Thole [13] were used. Since different charge distributions were employed in the quantum mechanical and classical approach, the absolute values of $\Delta G_{\mathrm{elst}}^{(f,f)}$ and their differences between *cis* and *trans* forms are consequently different. In spite of this, the general trend of solvant stabilization is preserved between MNU and ENU, as well as between *cis* and *trans* forms.

### 3.2. CALCULATIONS OF DISPERSION AND REPULSION SOLUTE–SOLVENT INTERACTION

The method of evaluating the Gibbs free energy of dispersion–repulsion, i.e. approximations A–E (see section 2, as well as the original paper [34] for details) was applied to a series of test molecules containing functional groups of diverse polarity and symmetry. The geometries of all test molecules were optimized using ab initio level (4-31G basis set) calculations. Atomic net charges from Mulliken's population analysis were used in the computation of the structure-dependent atomic Van der Waals radii and mean polarizabilities [34,56].

The dispersion–repulsion quantities (approximations A–E) for two series of polar and nonpolar solutes dissolved in a series of polar solvents ($H_2O$, $CH_3OH$ and $C_2H_5OH$) are shown in table 2. It can be seen from these data that the magnitudes of $\Delta G_{\mathrm{d,r}}$, obtained by means of approximations A and B, increase to too high values (absolute values) by increasing the size and the molecular polarizability of the solute and by increasing the size of the solvent molecule. Approximations C–E give $\Delta G_{\mathrm{d,r}}$ values that slightly increase as the effective radius of the solvent molecule increases. The relative trends in the $\Delta G_{\mathrm{d,r}}$ values can be compared for the two quasi-homologous series in different solvents by means of the reduced magnitudes $\Delta G_{\mathrm{d,r}}/N_1$ taken per one solvent molecule in the first solvation shell: e.g. in approximation E for methanol in three different solvents, the absolute values of $|\Delta G_{\mathrm{d,r}}/N_1|$ are 0.54 ($H_2O$) < 0.65 ($CH_3OH$) < 0.70 ($C_2H_5OH$) and for ethane, the values are 0.63 ($H_2O$) < 0.73 ($CH_3OH$) < 0.78 ($C_2H_5OH$). These values indicate that mean quantities $\Delta G_{\mathrm{d,r}}/N_1$ in approximation E follow a reasonable trend of increasing dispersion–repulsion interaction by increasing the size of the solvent molecules.

The relatively simple formulas based on the London and Born formulas are able to evaluate the solute–solvent dispersion–repulsion interactions. However, since the $\Delta G_{\mathrm{d-r}}$ values are not balanced with respect to other solute–solvent interaction contributions, it is better to consider just relative differences $\Delta\Delta G_{\mathrm{d-r}}$ within a series of solvents or solutes.

### 3.3. INTERPRETATION OF INTERPHASE PARTITIONING, CHROMATOGRAPHIC SEPARATION AND TRANSPORT THROUGH BOUNDARIES

As we have shown in section 2.2, continuum models of solvent effect can be used for the interpretation of the partition coefficient, the chromatographic

Table 2

The comparison of Gibbs free energies of dispersion–repulsion interactions ($\Delta G_{disp,rep}$), approximations A–E, for solutes in water, methanol and ethanol as solvents.

| Solute | $N_1$[a] | $\Delta G_{disp,rep}$ [kcal mol$^{-1}$] | | | | |
|---|---|---|---|---|---|---|
| | | A | B | C | D | E |
| *Water* | | | | | | |
| $H_2O$ | 9 | −4.21 | −4.62 | −3.40 | −4.43 | −4.26 |
| $CH_3OH$ | 12 | −13.38 | −7.65 | −5.22 | −7.12 | −6.82 |
| $CH_3OCH_3$ | 14 | −18.95 | −9.06 | −6.11 | −8.48 | −8.10 |
| $CH_4$ | 10 | −24.58 | −8.56 | −5.10 | −7.05 | −6.76 |
| $C_2H_6$ | 13 | −34.35 | −10.44 | −6.47 | −9.02 | −8.60 |
| $C_3H_8$ | 15 | −38.18 | −11.48 | −7.04 | −9.87 | −9.43 |
| *Methanol* | | | | | | |
| $H_2O$ | 7 | −6.29 | −6.52 | −2.79 | −3.92 | −3.74 |
| $CH_3OH$ | 9 | −22.48 | −11.07 | −4.18 | −6.23 | −5.95 |
| $CH_3OCH_3$ | 11 | −34.03 | −13.17 | −4.81 | −7.34 | −6.99 |
| $CH_4$ | 8 | −39.18 | −12.41 | −4.14 | −6.21 | −6.52 |
| $C_2H_6$ | 10 | −59.40 | −15.32 | −5.12 | −7.86 | −7.48 |
| $C_3H_8$ | 11 | −69.79 | −16.82 | −5.51 | −8.57 | −8.13 |
| *Ethanol* | | | | | | |
| $H_2O$ | 6 | −6.96 | −7.14 | −2.62 | −3.72 | −3.67 |
| $CH_3OH$ | 8 | −26.39 | −12.38 | −3.90 | −5.92 | −5.68 |
| $CH_3OCH_3$ | 10 | −41.34 | −14.80 | −4.44 | −6.95 | −6.69 |
| $CH_4$ | 7 | −44.07 | −13.89 | −3.88 | −5.92 | −5.67 |
| $C_2H_6$ | 9 | −70.87 | −17.29 | −4.74 | −7.45 | −7.11 |
| $C_3H_8$ | 10 | −85.73 | −19.05 | −5.07 | −8.12 | −7.74 |

[a] The packing number of solvent molecules in the first solvation shell.

separation, and the kinetics of transport through interphase boundaries. We have applied this approach to the calculation of $\Delta G_{solv}$ and consequently log $P$ and log $k$ for several series of compounds, namely hydrocarbons and their derivatives [57], polychlorinated biphenyls [29], a group of oxygen-containing compounds [30], and gas–liquid chromatography parameters of series of alkylbenzenes [46]. For several series (nitrosureas, nitrosoamines, 2-formylpyridine thiosemicarbazones) calculated values of $\Delta G_{solv}$ (and log $P$) have been used in structure–activity relationship studies [31,44]. Here we show an example of the calculation of the interphase partitioning characteristics of a series of fifteen polychlorated biphenyls (PCB) in a water/octanol system which is often used to simulate hydrophilic/lipophilic phase distribution of compounds in biosystems [58]. The theoretical values of the distribution coefficient log $P$ were calculated via the solvation Gibbs free energies in the two model liquids in the framework of the polarizable continuum model using a linear

regression of the $\Delta G_{solv}^{w,o}$ quantities with the experimental $\log P_{exp}$ values [29], which yields the correlation equation.

$$\log P = 0.301 \times \Delta G_{solv}^{w,o} + 0.24,, \qquad (30)$$

$$n=15,\ R=0.979,\ F=296.2,\ \alpha=99.99\%.$$

$n$ is the number of substances, $R$ the correlation coefficient, $F$ the statistical significance of the regression ($F$-test), and $\alpha$ is the level of statistical significance.

The individual contributions to the partitioning Gibbs free energy, as well as the log $P$ magnitudes, are given in table 3. We can see from the statistical parameters

Table 3

The contributions to the partitioning Gibbs free energies in a water/octanol system within the PCM model and log $P$ values for the series of polychlorinated biphenyls (in kcal/mol).

| X-PCB | $\Delta G_{elst}^{w,o}$ | $\Delta G_{d,r}^{w,o}$ | $\Delta G_{cav}^{w,o}$ | $\Delta G_{solv}^{w,o}$ | $\log P_{theor}$ [a] | $\log P_{exp}$ [b] |
|---|---|---|---|---|---|---|
| 2-Cl | − 0.216 | − 0.672 | 14.28 | 13.39 | 4.27 | 4.30 |
| 2,2'-Cl | − 0.403 | − 0.196 | 15.22 | 14.62 | 4.64 | 4.90 |
| 2,3'-Cl | − 0.407 | − 0.053 | 15.46 | 15.00 | 4.75 | 4.80 |
| 2,6'Cl | − 0.380 | − 0.078 | 15.23 | 14.77 | 4.68 | 5.00 |
| 2,3,2',3'-Cl | − 0.666 | 0.772 | 17.14 | 17.24 | 5.43 | 5.60 |
| 2,3,2',5'-Cl | − 0.331 | 1.077 | 17.28 | 18.02 | 5.66 | 6.00 |
| 3,4,3',4'-Cl | − 0.667 | 1.203 | 17.83 | 18.36 | 5.76 | 6.10 |
| 2,3,4,2,5-Cl | − 0.810 | 1.671 | 18.34 | 19.20 | 6.02 | 6.50 |
| biphenyl | − 0.246 | − 1.326 | 13.32 | 11.75 | 3.77 | 3.90 |
| 2,5,4'-Cl | − 0.716 | 0.640 | 16.69 | 16.61 | 5.24 | 5.70 |
| 2,4,4'-Cl | − 0.565 | 0.650 | 16.69 | 16.77 | 5.29 | 5.80 |
| 2,5,3',4'-Cl | − 0.648 | 1.220 | 17.74 | 18.24 | 5.73 | 5.90 |
| 2,4,2',5'-Cl | − 0.721 | 1.143 | 17.43 | 17.85 | 5.61 | 6.10 |
| 2,4,2',4'-Cl | − 0.722 | 1.168 | 17.44 | 17.89 | 5.62 | 5.90 |
| 2,5,2',5'-Cl | − 0.716 | 1.125 | 17.43 | 17.84 | 5.61 | 6.10 |

[a] Theoretical log $P$ values calculated according to eq. (30).
[b] Experimental log $P$ values (ref. [84]).

of the regression eq. (30) ($R$, $F$, $\alpha$) that the correlation is satisfactory and the theoretically evaluated $\log P_{theor}$ magnitudes are within an 8% error. The correlation eq. (30) can be used for the estimate of log $P$ values for other PCB derivatives. Such a theoretical approach to the distribution properties evaluation may be utilized in the case of any substances (e.g. also for unstable intermediates where experimental methods are not applicable).

Similarly, the energetic profile of the transport of several molecules through an electric bilayer forming at the boundary between octanol and water has been

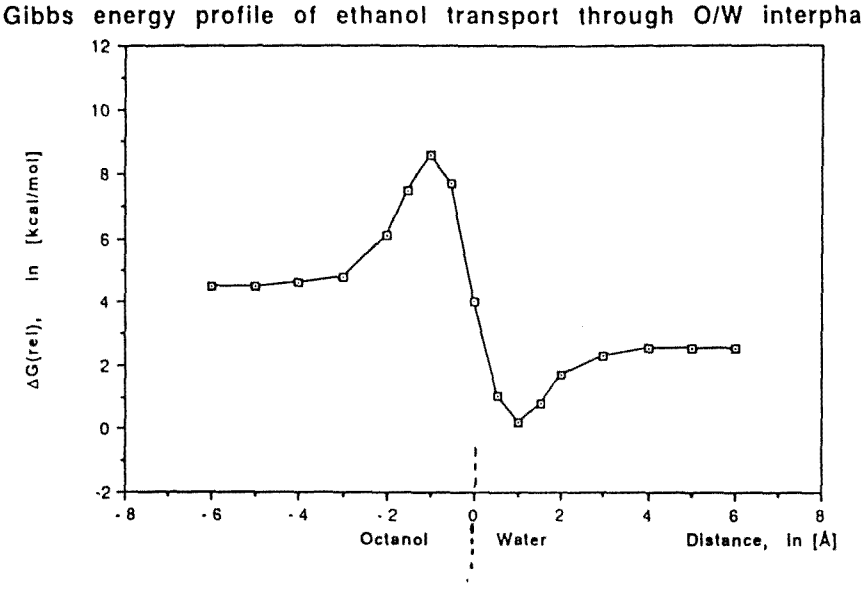


Fig. 2. Dependence of relative Gibbs energy of the system presented in fig. 1; $r_{rel} = 0$ on the graph corresponds to the structure designed in fig. 1.

calculated [43]. The model adopted is shown in fig. 1. In fig. 2 is shown the profile of $\Delta G$ calculated for the transport of ethanol through this boundary. Using the values from this curve, the partitioning of ethanol between both phases, as well as the rate of transport of solute from octanol to water and vice versa, can be calculated according to eqs. (27) and (28). This approach, focusing on the modelling of drug transport in biological systems, is now in progress [59].

## Acknowledgements

The authors are grateful to Michela Dario and Jan Miertus, Jr. for their assistance in the preparation of this manuscript.

## References

[1] A. Warshel and S.T. Russell, Quart. Rev. Biophys. 17(1984)78.
[2] K.N. Swamy and E. Clementi, in: *Structure and Dyanmics of Proteins, Nucleic Acids and Membranes*, ed. E. Clementi and S. Chin (Plenum, New York, 1986).
[3] S. Miertus, V. Frecer and M. Majekova, Interpretation and prediction of biochemical process at molecular level, in: *Theoretical Biochemistry and Biophysics: A Computational Survey*, ed. D.L. Beveridge and R. Lavery (Adenine Press, New York, 1990), p. 131.
[4] A. Pullman and B. Pullman, Quart. Rev. Biophys. 7(175)505.
[5] J.O. Noell and K. Morokuma, J. Phys. Chem. 80(1976)2675.
[6] B. Pullman, S. Miertus and C. Perahia, Theor. Chim. Acta 50(1979)317.

[7] (a) M.J. Huron and P. Claverie, J. Phys. Chem. 76(1972)2133; 78(1974)1853; 78(1974)1862;
(b) J. Langlet, P. Claverie, J. Caillet and A. Pullman, J. Phys. Chem. 92(1988)1617;
(c) R. Constanciel, Theor. Chim. Acta 69(1986)505.
[8] (a) O. Tapia and O. Goscinski, Mol. Phys. 29(1975)1653;
(b) J.L. Rivail and D. Rinaldi, Chem. Phys. 18(1976)233.
[9] B.T. Thole and P.Th. van Duijnen, Chem. Phys. 71(1982)211.
[10] S. Miertus, E. Scrocco and J. Tomasi, Chem. Phys. 55(1981)117.
[11] S. Miertus and J. Tomasi, Chem. Phys. 65(1982)238.
[12] S. Miertus, V. Frecer and M. Majekova, J. Mol. Struct. (THEOCHEM) 179(1988)353.
[13] A. Warshel and M. Levitt, J. Mol. Biol. 103(1976)227.
[14] B. Jayaram, K. Sharp and B. Honig, Biopolymers 28(1989)975.
[15] H. Sklenar, F. Eisenhaber, M. Poncin and R. Lavery, in: *Theoretical Biochemistry and Biophysics: A Comparative Survey, ed. D.L. Beveridge and R. Lavery* (Adenine Press, New York, 1990), 9.239.
[16] C.E. Felder and J. Applequist, J. Chem. Phys. 75(1981)2390.
[17] (a) W.H. Orttung and D. Vosooghi, J. Phys. Chem. 87(1983)1432;
(b) A.A. Rashin and K. Namboodiri, J. Phys. Chem. 91(1987)6003;
(c) R.J. Zauhar and R.S. Morgan, J. Comput. Chem. 9(1988)171.
[18] V. Frecer and S. Miertus, Int. J. Quant. Chem. 42(1992),
[19] E. Clementi, *Computational Aspects for Large Systems,* Lecture Notes in Chemistry, Vol. 19, ed. G. Berthier et al. (Springer, New York, 1980), p. 74.
[20] K.N. Swamy and E. Clementi, in: *Structure and Dynamics of Proteins, Nucleic Acids and Membranes,* ed. E. Clementi and S. Chin (Plenum, New York, 1986), p. 219.
[21] W.L. Jorgensen and C. Ravimohan, J. Chem. Phys. 83(1985)3050.
[22] J.A. McCammon and M. Karplus, Ann. Rev. Phys. Chem. 31(1980)29.
[23] C.F. Wong and J.A. McCammon, J. Amer. Chem. Soc. 108(1986)3830.
[24] M. Mezei, P.K. Mehrota and D.L. Beveridge, J. Amer. Chem. Soc. 107(1985)2239.
[25] A. Warshel, Proc. Nat. Acad. Sci. USA 81(1984)58.
[26] W.L. Jorgensen and J.K. Buckner, J. Phys. Chem. 91(1987)6083.
[27] (a) P.A. Bash, U.C. Singh, R. Langridge and P.A. Kollman, Science 236(1987)564;
(b) D.L. Beveridge and F.M. DiCapua, Ann. Rev. Biophys. Biophys. Chem. 18(1989)431;
(c) A. Warshel et al., J. Phys. Chem. 86(1982)2218;
(d) A. Warshel et al., Pontif. Acad. Script. Var. 55(1984)59;
(e) A. Warshel, J. Phys. Chem. 83(1979)1640.
[28] (a) E. Cimiraglia, S. Miertus and J. Tomasi, Chem. Phys. Lett. 80(1981)286;
(b) P. Claverie, J.P. Daudey, J. Langlet and B. Piazzolla, J. Chem. Phys. 82(1978)405;
(c) G.W. Schnuelle and D.L. Beveridge, J. Phys. Chem. 79(1975)2566.
[29] S. Miertus and V. Jakus, Chem. Zvesti 44(1990)354.
[30] S. Miertus and R. Moravek, Coll. Czech-Slov. Chem. Commun. 55(1990)2430.
[31] S. Miertus, V. Frecer and M. Majekova, Int. J. Quant. Chem. 35(1989)153.
[32] O.S. Ventura, A. Liedos, R. Bonnaccorsi, I. Bertran and J. Tomasi, Theor. Chim. Acta (Berlin) 72(1987)175.
[33] J. Tomasi, G. Alagona, R. Bonaccorsi and C. Ghio, in: *Modelling of Structures and Properties of Molecules,* ed. Z. Maksic (Horwood, Chichester, 1987).
[34] V. Frecer, S. Miertus and M. Majekova, J. Mol. Struct. (THEOCHEM) 216(1991)312.
[35] F. Floris and J. Tomasi, J. Comput. Chem. 10(1989)616.
[36] F. London, Z. Phys. 633(1980)245.
[37] F. London, Trans. Faraday Soc. 33(1937)8.
[38] F. London, Z. Phys. Chem. Abt. B311(1930)222.
[39] M. Born and J. Mayer, Z. Phys. 75(1932)1.
[40] J.M. Huron and P. Claverie, J. Chem. Phys. 76(1972)2123.
[41] R.A. Pierotti, J. Phys. Chem. 67(1963)1840; 69(1965)281.

[42] O. Sinanoglu and O. Halicioglu, Ann. NY Acad. Sci. 158(1969)308.
[43] V. Frecer and S. Miertus, J. Mol. Struct. (THEOCHEM), to be published.
[44] V. Frecer and S. Miertus, Neoplasma 35(1988)252; 36(1989)257.
[45] R. Bonaccorsi, F. Floris, P. Palla and J. Tomasi, Thermochim. Acta 162(1990)213.
[46] S. Miertus, V. Jakus and M. Matisova, Chromatographia 30(1990)144.
[47] S. Miertus and V. Jakus, Chromatography, submitted for publication.
[48] H. Hoshi, M. Sakurai, Y. Inoue and R. Chujo, J. Chem. Phys. 87(1987)1107.
[49] R. Bonaccorsi, R. Cimiraglia, J. Tomasi and S. Miertus, J. Mol. Struct. (THEOCHEM) 94(1983)11.
[50] R. Bonaccorsi, R. Cammi and J. Tomasi, J. Comp. Chem. (1991), in press.
[51] H. Weinstein, R. Osman, L. Pardo and S. Miertus, unpublished results.
[52] A. Warshel, F. Sussman and J. King, Biochem. 25(1986)8368.
[53] S. Miertus and V. Frecer, Biophys. Chem., in preparation.
[54] S.J. Weiner, P.A. Kollman, D.A. Case, U.C. Singh, C. Ghio, G. Alagona, S. Profeta, Jr. and P. Weiner, J. Amer. Chem. Soc. 106(1984)765.
[55] M.L. Connolly, J. Appl. Cryst. 16(1983)548.
[56] S. Miertus, J. Bartos and M. Trebaticka, J. Mol. Liquids 33(1987)139.
[57] S. Miertus, V. Frecer, M. Trebaticka and V. Jakus, in: *QSAR in Toxicology and Xenobiochemistry*, ed. M. Tichy (Elsevier, Amsterdam, 1985).
[58] C. Hansch and W.J. Dunn, J. Pharm. Sci. 61(1972)7.
[59] S. Miertus and V. Frecer, J. Mol. Struct. (THEOCHEM), in preparation.
[60] (a) O. Jano, Comp. Rend. Acad. Sci. (Paris) 261(1965)103;
(b) S. Miertus and O. Kysel, Chem. Phys. Lett. 65(1979)395;
(c) S. Miertus, O. Kysel and O. Krejci, Chem. Papers 35(1981)3.
[61] G. Klopman, Chem. Phys. Lett. 1(1967)200.
[62] (a) S. Miertus and O. Kysel, Chem. Phys. 21(1977)27, 33;
(b) R. Contreras and J.S. Jeria, J. Phys. Chem. 88(1988)1905.
[63] V. Frecer, M. Majekova and S. Miertus, J. Mol. Struct. (THEOCHEM) 183(1989)403.
[64] M.N. Bellido and J.A.C. Rullmann, J. Comput. Chem. 10(1989)479.
[65] (a) B.Th. Thole, Chem. Phys. 59(1981)341;
(b) J.A.C. Rullmann, M.N. Bellido and P.Th. van Duijnen, J. Mol. Biol. 206(1989)101, and refs. therein;
(c) G.A. Mercier, Jr., J.P. Dijkman, R. Osman and H. Weinstein, Effects of macromolecular environment on proton transfer process: The calculation of polarization, in: *Quantum Chemistry – Basic Aspects, Actual Trends*, ed. R. Carbo, Studies in Physical and Theoretical Chemistry, Vol. 62 (1988) p. 577.
[66] A. Bondi, J. Phys. Chem. 68(1964)441.
[67] R. Bonaccorsi, F. Floris and J. Tomasi, J. Mol. Liquids 47(1990)25.
[68] S. Miertus, O. Incani and N. Rahman, J. Mol. Struct. (THEOCHEM), in preparation.
[69] R. Montagnani and J. Tomasi, Int. J. Quant. Chem., in press.
[70] H.J. Hofmann, R. Cimiraglia, R. Bonaccorsi and J. Tomasi, Eur. J. Med. Chem. 25(1990)127.
[71] J. Tomasi et al., Chem. Phys., in preparation.
[72] R. Cammi, F.J. Olivares and J. Tomasi, Chem. Phys. 122(1988)63.
[73] R. Bonaccorsi, E. Ojalvo and J. Tomasi, Coll. Czech-Slov. Commun. 53(1988)2320
[74] R. Bonaccorsi, E. Ojalvo, P. Palla and J. Tomasi, Chem. Phys. 143(1990)245.
[75] R. Bonaccorsi, J. Tomasi, C.A. Reynolds and C. Thomson, J. Comput. Chem. 9(1988)779.
[76] S. Miertus and M. Trebaticka, J. Theor. Bio. 108(1984)509.
[77] B.J. Yoon and A.M. Lenhoff, J. Comput. Chem. 11(1990)1080.
[78] K.A. Sharp and B. Honig, Ann. Rev. Biophys. Chem. 19(1990)301.
[79] F.J. Olivares del Valle and M. Aguilar, J. Comput. Chem. 10(1989)432.
[80] C. Giessner-Prettre and A. Pullman, Theor. Chim. Acta 25(1972)83.
[81] M.J.S. Dewar, E.G. Zoebisch, E.F. Healy and J.J.P. Stewart, J. Amer. Chem. Soc. 107(1985)3902.
[82] R. Bianco, S. Miertus, M. Persico and J. Tomasi, Chem. Phys., in press.
[83] M. Aguilar, S. Miertus, M. Persico and J. Tomasi, in preparation.
[84] W.Y. Shiw and D. Mackay, J. Phys. Chem. Ref. Data 15(1986)911.